Rotational and Penetration Rate Effects on the Formation and Axial Capacity of Pressure-Grouted Helical Piles

Qiang Wang[1], Fu Yang[2], Shuai Fang[2*], Yucun Yang[3], Wei Zhang[3], Jinlong Zhang[3]

[1] Jiangsu Qitian Electric Power Construction Group CO., LTD., Lianyungang, China
[2] Lianyungang Zhiyuan Electric Power Design CO., LTD., Lianyungang, China
[3] Jiangsu Huiwen Electric Power Engineering CO., LTD., Nanjing, China

Abstract: The Pressure Grouted Helical Pile (PGHP) is an innovative composite foundation system built in one step by combining the structural stiffness of a helical shaft and the deformability of a cement treated pile body. This system of - high installation efficiency, high structural integrity and improved pile - soil interface bonding - has demonstrated wide-spread application potential in geotechnical engineering. In order to systematically investigate its formation process and load-bearing behavior, 6 groups with 24 model piles were tested under simulated marine soft clay conditions. The research examined the effects of the major construction variables, such as rotational velocity and penetration rate on pile diameter, axial load-bearing capacity and mechanics of the cement stabilized soil. The increases in rotation speed between moderates and excessive increases increase the uniformity of the soil-cement and pile integrity, while excessively high speeds decrease the grout intake, resulting in smaller pile diameters and weaker strength. This study explains the mechanisms by which the construction parameters control the formation and performance of PGHPs, which not only shed light on the formation of PGHPs but also offer practical information for the design optimization and engineering application of PGHPs.

1 Introduction

The Pressure Grouted Helical Pile (PGHP) is a novel type of composite foundation element, which is designed and produced in a single construction process and combines a rigid helical shaft with a deformable pile body that is cement treated. This innovative configuration mani-fests several prominent advantages, including superior construction efficiency, enhanced pile integrity, reliable pile-soil interfacial bonding and excellent long-term durability [1]. Existing research has corroborated that PGHPs not only significantly enhance the ultimate bearing capacity and initial stiffness of pile foundations, but also enhance the homogeneity of surrounding cemented soil and reduce the environmental disturbances caused by construction, thereby significantly reinforcing the overall effectiveness of ground improvement [2]. To date PGHPs have already been implemented in a number of engineering practices, showing promising potential for wider application [3].

From a scholarly point of view both domestic and international scholars have conducted systematic research on helical piles and stiffened composite piles. Rao [4] Lutenegger [5] and Merrifield [6] based on field testing and finite element analysis, comprehensively analyzed the effect of blade number, spacing ratio and embedment depth on the vertical bearing capacity of helical piles, and further proposed a series of theoretical calculation frameworks. Complementary numerical simulations have been used to elucidate the intrinsic correlations between load-bearing behavior and governing geometric parameters and develop predictive models for single-pile ultimate capacity [7]. Such findings together provide a solid theoretical underpinning for the further development and engineering application of PGHPs.

In relation to PGHPs specifically, exploratory model tests and numerical analyses have also been carried out. Nabizadeh [8, 9] proved that suitable in-crease in the number of blades can significantly improve the overall performance of the pile, although an excessive number of blades can aggravate the soil disturbance and hence reduce the overall bearing efficiency. Subsequent numerical analyses have indicated that the load-bearing capacity of PGHPs is around 1.5-2.2 *times* higher than the conventional jet-grouted piles, thus confirming the pronounced superiority of this composite system in terms of pile-soil interaction and pile integrity [10].

At the construction-technology level, Mansour [11] and colleagues revealed that grouting pressure and water-cement ratio have the decisive influences on the strength development of cemented soil around the pile. Proper adjustment of these parameters has been shown to not only increase the ultimate load bearing capacity of the pile but also increase the uniformity of the mechanical properties within the cement stabilized soil mass [12].

The above mentioned achievements have further supported the engineering viability of PGHPs and at the same time provided theoretical knowledge and practical guidance for the optimization of other composite pile systems.

*Corresponding Author Email: 188996383@qq.com

Nonetheless, most of the existing studies are still restricted to isolated parametric analyses and systematic experimental investigations with regard to critical construction parameters, rotation speed and penetration speed are still missing. Against this background, in the present study PGHPs are taken as the object of study and a series of controlled laboratory model tests are carried out. By combining load-displacement curve analysis and nail-shooting strength tests, the study systematically analyzes the effects of the above-mentioned parameters on the formation quality of piles, vertical load-bearing behavior, and the strength of surrounding cemented soil, and reveals the corresponding mechanisms. On the basis of this, optimization strategies and appropriate parameter ranges for PGHP construction are proposed. The outcomes of this work are expected to provide meaningful theoretical enrichment, methodological refinement, and engineering reference for the broader application and optimization of PGHP technology.

2 Experimental Program

2.1 Soil Properties

The kaolin dry powder is illustrated in Fig. 1, and its chemical composition is presented in Table 1. In accordance with the *Specifications for Geotechnical Testing of Highway Engineering* (JTG 3430, 2020), the liquid and plastic limits of kaolin were determined using the cone penetration method. The relationship between cone penetration depth (76 *g*) and water content is shown in Fig. 2. The basic physical properties of kaolin are summarized in Table 2. The particle-size distribution curve is provided in Fig. 3, indicating a relatively smooth gradation, uniform particle size, and satisfactory distribution characteristics.

Table 1. The main chemical composition of kaolin (*%*)

SiO_2	Al_2O_3	Fe_2O_3	MgO	CaO	Na_2O	K_2O	TiO_2	MnO	P_2O_5	SO_3	loss on ignition
70.158	18.994	0.375	0.198	0.244	0.899	2.4	0.041	0.037	0.037	0.066	6.52

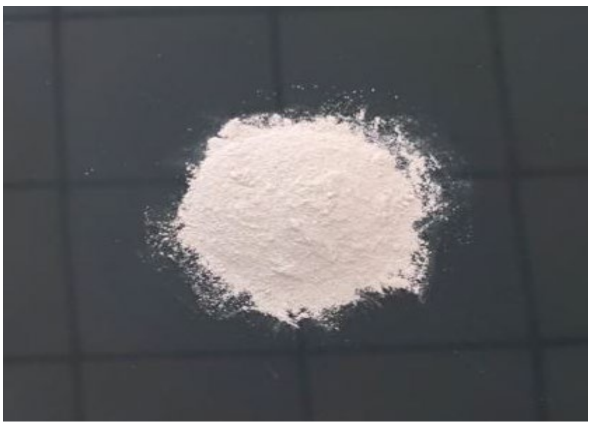

Fig. 1. Dry kaolin powder

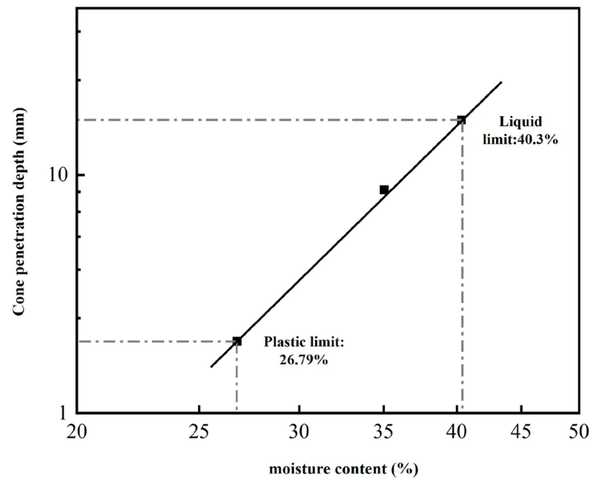

Fig. 2. Cone penetration depth–water content

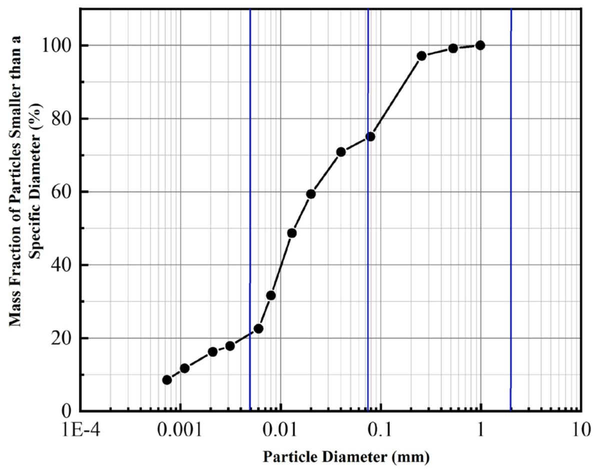

Fig. 3. Aggregation curve of kaolin particles particles

Table 2. Physical performance index table

Relative Density	Liquid Limit	Plastic Limit	Plasticity Index
2.536	40.36	26.79	13.57

A mixer was used to prepare the experimental soil. For the preparation of the experimental soil, 10 *L* of water was added per 20 *kg* of soil for mixing. The mixing duration with the mechanical mixer should not be less than 40 *minutes* to ensure the uniformity of the experimental soil. After the mixing duration, the soil was extracted and filtered through a 3 *mm* stainless steel sieve to remove impurities, thus completing the preparation of the experimental soil.

After preparation, the experimental soil undergoes a drainage consolidation process for 28 *days*. During this period, the water content of the soil decreases to 45%–50%, and the undrained shear strength reaches 1.0–2.0 *kPa*. When the soil's properties are similar to those of marine soft soil, pile-driving tests are conducted. For this purpose, the T-bar method was used to assess the undrained shear strength of the soil, with the results presented in Figure 4.

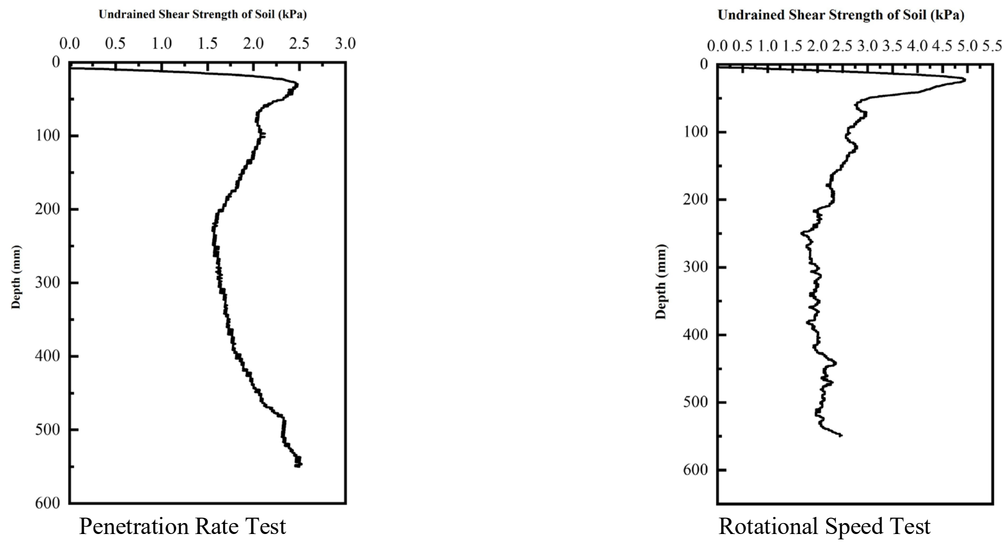

Fig. 4. Undrained shear strength curve

2.2 Experimental Equipment and Pile Model

The experimental geotechnical box has dimensions of 2100 *mm* × 800 *mm* × 1100 *mm*, constructed from transparent acrylic panels and stainless steel square tubes, with internal seams sealed using silicone sealant to prevent leakage. Four rollers are installed at the base of the geotechnical box to facilitate positioning adjustments.

As shown in Figure 5, the pile installation equipment used in the PGHP synchronous spiral grouting technique consists of a control console, grouting system, and rotary pile system. The core pile in the PGHP system is a steel pipe helical pile, which is fabricated from steel. The helical blade has a diameter of D_H=66*mm*, and the central steel pipe has a diameter of D_S=22*mm*. The pile length is L_S=600*mm*, with a spiral blade pitch S=160*mm*. The length of the pile body above the first layer of blades is h_1=100*mm*, and the length of the pile body below the bottom layer of blades is h_2=20*mm*. The blade pitch is 22.5 *mm*. Given that the typical dimensions are a central pipe diameter of 89 mm and a helical blade diameter of 260 mm, this study performs a scaled experiment with a scale ratio of 4. To minimize disturbance to the surrounding soil during pile installation, the openings in the helical blades are welded along a continuous line. The structural configuration of the helical pile body is depicted in Figure 6.

Fig. 5. Rotary pile system

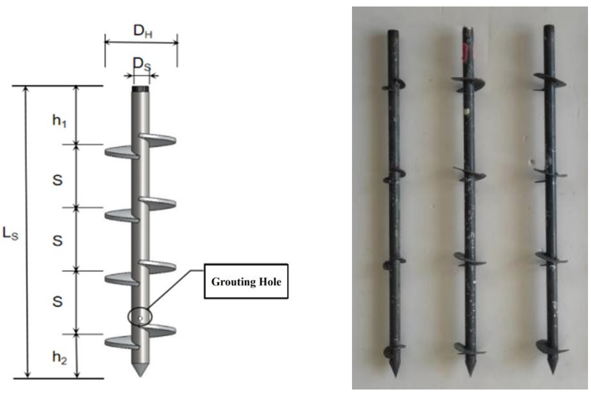

Fig. 6. Helical piles for PGHPs

2.3 Experimental Equipment and Pile Model

2.3.1 Experimental Design

The detailed experimental parameters for the model piles are presented in Table 3. During the laboratory installation process, the model piles were placed vertically and at equal intervals within the geotechnical container, maintaining a distance of 350 mm between each pile and the adjacent inner walls of the box. The lateral influence of the piles on the surrounding soil was confined to an area where the effect was considered negligible, defined as three times the pile diameter, thereby mitigating boundary effects.

Pressure grouting was performed using a diaphragm pump (Model GP-25), rated to 20 L min^{-1}, connected via a 10 mm-ID grout hose of length 3.0 m with an inline check valve positioned 0.5 m upstream of the injection port. Inline pressure (0–1.6 MPa, ±0.5 % FS) and turbine flow (0–25 L min^{-1}, ±1.0 % RD) transducers (Models PT-1600 and TF-25, respectively) were calibrated within 30 days prior to testing and logged at 5 Hz together with rotational speed and penetration rate. The grout comprised P·O 42.5R cement with water–cement ratio w/c=0.70 and a polycarboxylate superplasticizer at 0.8 % by cement mass. Target slurry density and Marsh funnel time were 1.75 ± 0.02 g cm^{-3} and 35 ± 3 s, respectively, verified per batch at 20 ± 2 °C. Water, admixture, and cement were combined in a 2.2 kW high-shear mixer for 2 min, rested for 1 min, and re-mixed for 1 min before pumping; batches standing more than 10 min were re-agitated for 30 s. Batches were accepted when density and Marsh time met targets and when steady-state pressure fluctuations were < 0.010 MPa over 10 s. Installation segments were accepted when 0.80 $\leq R_g \leq$ 1.1, otherwise drilling was paused and parameters adjusted.

2.3.2 Loading Scheme

Following the pile installation test, vertical loading tests were performed after the cement-soil mixture had consolidated and set for 7 *days*. As shown in Figure 7, to record the displacement at the pile head, a displacement transducer was installed directly beneath the loading plate. Since the load plate could not be perfectly level, minor tilting was possible. To address this, three displacement sensors were placed beneath the load plate, and the average of the three readings was used as the displacement value of the pile body.

Table 3. Table of Model Pile Test Parameters

Test Group	Code	Water-to-Cement Ratio (*w/c*)	Grouting Pressure (*MPa*)	Penetration Rate (*cm/min*)	Rotational Speed (*rad/min*)	Number of Blades (*pieces*)
Rotational Speed	PGHP-RS-1	0.6	.0.2	20	8	4
	PGHP-RS-2				16	
	PGHP-RS-3				32	
Penetration Speed	PGHP-DS-1	0.6	0.2	20	13.2	4
	PGHP-DS-2			30	19.8	
	PGHP-DS-3			40	264	

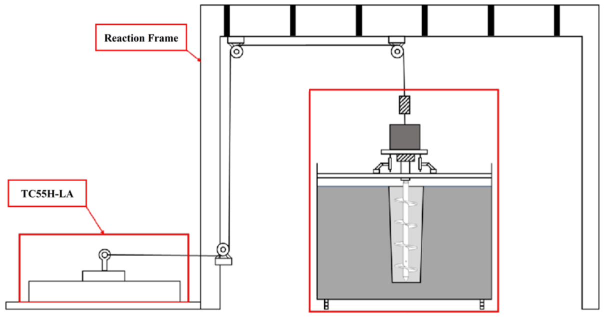

Fig. 7. Loading test

2.3.3 Cement-Soil Strength Detection of the Pile Body

The cement-soil strength of the pile body was tested after the loading experiment. To minimize damage to the pile body, the stud method (nail-in method) was chosen to detect the cement-soil strength around the pile. The stud device used in this experiment was a gas-powered nail gun (Model 45S). The gas nail gun was used to insert standard nails into the cement-soil surrounding the pile. The length of the nails used was 30 *mm*, and the penetration depth of the nails was correlated with the cement-soil strength of the pile body. A relationship curve was established through the experiment (the relationship formula is shown in Equation (1) to calculate the cement-soil strength around the pile.

To improve the accuracy of the test results, five nails were inserted into each PGHP pile, evenly distributed along the pile body and arranged in a straight line. The nail points were numbered sequentially as A, B, C, D, and E. The arrangement of the nail points is shown in Figure 9.

The cement-soil strength detection equipment is shown in Figure 8.

$$Q_u = \left(\frac{T}{17.711}\right)^{\frac{1}{0.3037}} \tag{1}$$

In the formula:

Q_u represents the compressive strength of the cement-soil (*MPa*)

T represents the remaining penetration depth of the stud (*N*)

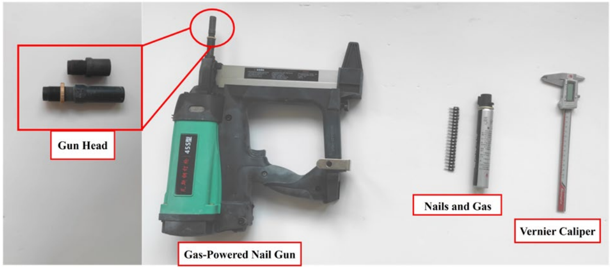

Fig. 8. Nail shooting test equipment

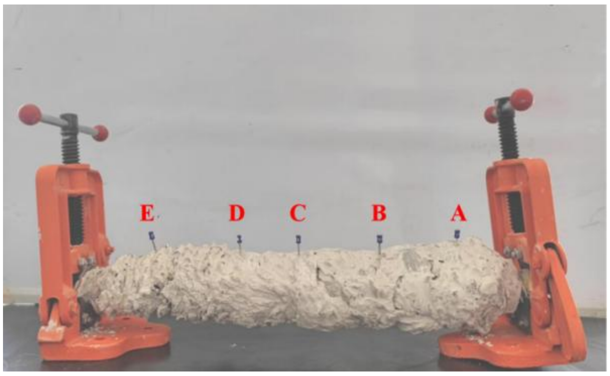

Fig. 9. Layout of nail point

3 PGHP Process Parameter Test Results and Analysis

3.1 Rotational Speed

3.1.1 Analysis of Rotational Speed on Pile Installation Effectiveness

The PGHP pile installation resulted in three model piles, all of which exhibited a frustum shape. For the rotational speed test groups (8, 16, and 32 *rad/min*), all three PGHP model piles exhibited a frustum shape. The PGHP-RS-16 and PGHP-RS-32 piles retained their structural integrity with smooth surfaces and no apparent cracks. In contrast, the PGHP-RS-1 pile showed surface cracks and a large amount of layering, indicating that a higher rotational speed plays a role in achieving a more compact and uniform pile formation. After the rotation-al loading test, the diameters of the PGHP model piles at the five typical sections (A-E) were measured at different rotational speeds (8, 16, 32 *rad/min*), and the results are presented in Table 4. The average diameters D_{AV} for PGHP-RS-1, PGHP-RS-2, and PGHP-RS-3 were 87.95 *mm*, 88.52 *mm*, and 81.25 *mm*, respectively. The average diameters of PGHP-RS-1 and PGHP-RS-2 were similar, indicating that the rotational speed had a negligible effect on the average pile diameter within the range of 8 *rad/min* to 16 *rad/min*. Raising the rotation rate from 8 to 16 rad·min^{-1} markedly reduced diameter variability and produced a substantially more uniform pile body. However, when the rotational speed was further increased to 32 *rad/min*, the uniformity of the pile diameter did not change significantly, indicating that the mixing action during the pile installation process had already been nearly sufficient.

To elucidate diameter variability, rotation-rate effects were evaluated by plotting diameter profiles at designated measurement locations for PGHP-RS-1, PGHP-RS-2, and PGHP-RS-3 (Figure 10). Measurements taken at multiple locations along the same pile reveal pronounced diameter fluctuations, with the largest value at point C and the smallest at point E. Such differences are attributable to the soil's density and shear strength across strata: in the middle layer, where compaction is moderate and shear resistance is relatively low, the grout diffuses more readily. Conversely, in the bottom layer, the higher shear strength and reduced splitting radius hinder grout penetration, producing a smaller pile diameter near the pile tip.

Table 4. Measured diameters for PGHPs with different rotary speed

Code	Diameters along PGHPs					DAV (mm)	$\frac{D_{max}-D_{\min}}{D_{\min}}$ (%)
	D_A *(mm)*	D_B *(mm)*	D_c *(mm)*	D_D *(mm)*	D_E *(mm)*		
PGHP-RS-1	80.64	91.89	97.53	92.23	77.32	87.95	26
PGHP-RS-2	86.85	87.8	104.28	87.30	76.05	88.52	17
PGHP-RS-3	81.87	83.77	91.66	72.2	78.87	81.25	16

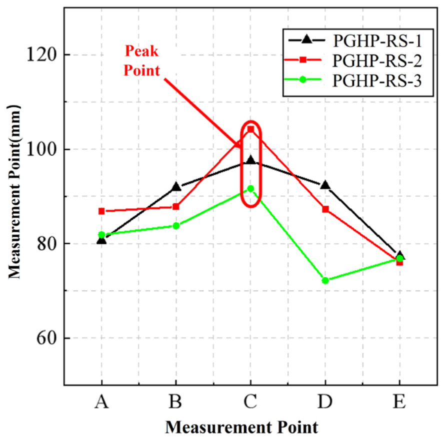

Fig. 10. Diameters measured for the PGHPs with different rotary speeds

3.1.2 Analysis of Rotational Speed on Vertical Bearing Capacity

Figure 11 shows the load-displacement curves for the rotational speed test groups. From Figure 11, it is evident that the overall curves consist of three stages: the initial elastic stage, the nonlinear plastic deformation stage, and the failure stage. The ultimate compressive bearing capacity of the PGHP piles in this batch lies at the end of the nonlinear stage.

Curve analysis reveals that both PGHP-RS-1 and PGHP-RS-3 experienced a significant decrease in bearing capacity after reaching the peak value. This is primarily due to the fact that these two piles were positioned near the sides of the geotechnical box, where a localized hard shell layer existed in the surface layer of the soil near the sidewalls. During the loading process, the lower part of the piles experienced concentrated stress, causing brittle failure of the local soil, which in turn weakened the pile foundation's bearing performance.

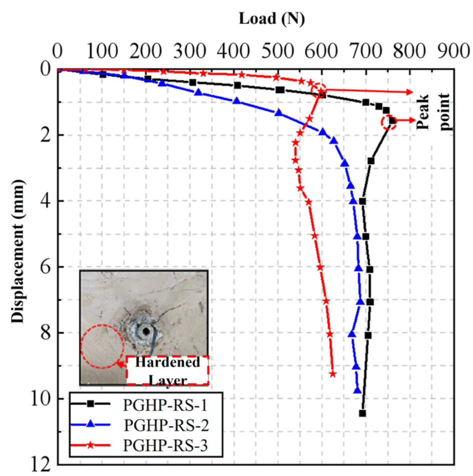

Fig. 11. The load-displacement curve of the rotation speed test group

The results of the ultimate compressive bearing capacity are shown in Table 5. PGHP-RS-1 exhibited the highest ultimate bearing capacity (725 *N*, displacement 1.23 *mm*), which was approximately 16% higher than PGHP-RS-2 (621 *N*) and 25% higher than PGHP-RS-3 (576 *N*).

Considering the pile diameter measurements, it was found that PGHP-RS-1 had a smaller average diameter, resulting in a relatively larger frictional surface area with the surrounding soil. This led to a higher contribution from the pile's surrounding skin friction, thus achieving the highest bearing capacity. In contrast, the PGHP-RS-3 pile exhibited a distinct helical structure around the pile body, which, combined with additional mechanical compressive stress, caused local failure of the surrounding soil. This resulted in the lowest ultimate bearing capacity for PGHP-RS-3.

Table 5. The ultimate bearing capacity of the test pile in the rotation speed test group

Code	Compressive Ultimate Bearing Capacity Pult (*N*)	Displacement (*mm*)
PGHP-RS-1	725	1.23
PGHP-RS-2	621	2.21
PGHP-RS-3	576	0.91

3.1.3 Rotational Speed on Cement-Soil Strength of PGHPs

The strength of soil-cement surrounding the pile was evaluated after extracting the pile using a stud-assisted procedure designed to limit disturbance to the specimen. Results for the series of rotational speeds are given in Figure 12.

Inspection of stud readings at several locations along a given pile shows pronounced spatial variability in strength. With more embedment, there is a tendency for strength to decrease and magnitude of fluctuation is not regular. This behavior is attributed to the difficulty of maintaining uniform pile quality under laboratory installation conditions and hence reduced, and less uniform, cement-soil strength at greater depths.

Cross-comparison of the three groups of rotation rates shows that the higher the rotational velocities, the more even the strength field around the pile and the smaller the fluctuation ranges. When the rate reached 16 rad/min, the variability effectively leveled off; further increases produced only marginal additional benefit. These observations suggest that a moderate increase in rotation improves mixing uniformity in the cemented soil annulus, thereby promoting a more homogeneous strength distribution along the pile.

Table 6 summarizes the cement-soil strength outcomes for the rotational-speed tests. The mean strength *(S_{AV})* for PGHP-RS-1, PGHP-RS-2, and PGHP-RS-3 is 2.762 MPa, 2.812 MPa, and 2.912 MPa, respectively. The data show that rotational speed has little influence on the average strength around the pile. This is expected because altering the rotation rate did not change the injected grout quantity; consequently, the cement dosage for all three model piles was identical, leading to negligible differences in mean cement-soil strength.

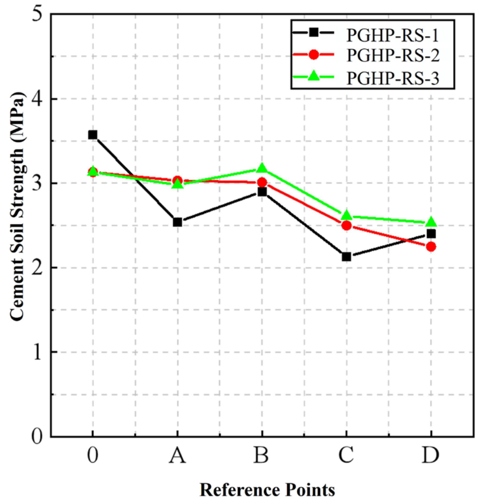

Fig. 12. Diagram for soil-cement strength along PGHPs with different rotating speed

Table 6. Results of PGHPs in the rotational speed test group

Code	Pile Diameter at Different Positions					S_{AV} (*mm*)
	S_A *(MPa)*	S_B *(MPa)*	S_C *(MPa)*	S_D *(MPa)*	S_E *(MPa)*	
PGHP-RS-1	3.62	2.59	2.95	2.17	2.44	2.762
PGHP-RS-2	3.19	3.06	3.04	2.52	2.29	2.812
PGHP-RS-3	3.17	3.00	3.20	2.63	2.55	2.902

3.2 Penetration Speed

3.2.1 Analysis of Penetration Speed on Pile Installation Effectiveness

Figure 13 presents the installation outcomes for the Penetration-rate series. The three specimens, PGHP-DS-1, PGHP-DS-2, and PGHP-DS-3, were installed at Penetration rates of 20, 30, and 40 mm·min^{-1}, respectively. Under different Penetration speed conditions, the diameter differences between the three piles were relatively small, but significant differences were observed in their surface morphology and cement-soil compaction. The PGHP-DS-1 pile had a rough surface, and clear helical structures were visible at the bottom. The pile showed a good bond with the surrounding soil. In contrast, the PGHP-DS-3 pile had a smooth and well-formed surface, but its diameter was slightly smaller than the other two piles.

These differences indicate that while the Penetration speed had minimal impact on the pile diameter, it significantly influenced the surface texture and compaction of the cement-soil around the pile. At the lowest penetration rate (PGHP-DS-1), the pile showed stronger interface adhesion with the surrounding soil. In contrast, the highest rate (PGHP-DS-3) produced a smoother and more uniform surface, accompanied by a smaller diameter.

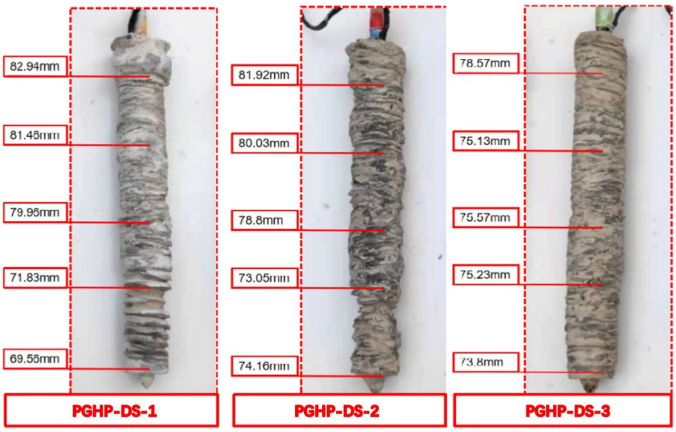

Fig. 13. Pictures of PGHPs with different

The diameter outcomes for the Penetration-rate series are summarized as follows. The mean diameters D_{AV} for PGHP-DS-1, PGHP-DS-2, and PGHP-DS-3 were 77.92 mm, 78.36mm, and 76.39mm, respectively, with the DS-40 specimen exhibiting a modestly smaller size than the other two. This reduction is attributed to the higher penetration rate, which curtailed grout intake and consequently lowered the cement slurry around the PGHPs.

The spreads between the maximum and minimum diameters were 19%, 13%, and 15% for DS-1, DS-2, and DS-3, indicating that the intermediate rate (30 mm·min^{-1}) produced the most uniform diameter. To elucidate the rate effect, diameter profiles at designated measurement points for DS-1, DS-2, and DS-3 were plotted (Figure 14). At 20 and 30 mm·min^{-1}, diameters generally tapered with depth, showing a pronounced drop at location D, yielding a frustum-like geometry. When the rate was increased from 30 to 40 mm. min^{-1} the amplitude of diameter fluctua-tions at the five points decreased.

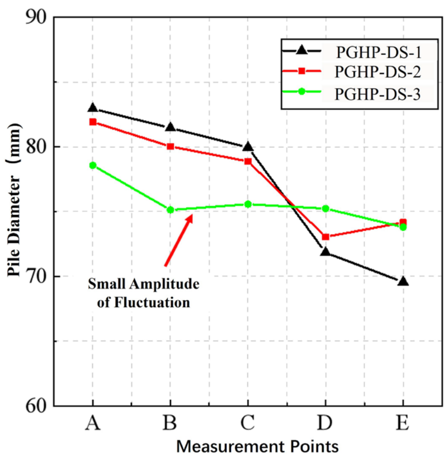

Fig. 14. Measured Diameters for the PGHPs with different penetration speed.

Grouting volumes were 2.89 L and 2.45 L for DS-1 and DS-2, respectively, while the corresponding average diameters differed only slightly, implying that, once grout supply is adequate, further slowing the Penetration (and thereby admitting more grout) exerts limited influence on diameter. By contrast, raising the rate from 30 to 40 mm·min^{-1} reduced grout uptake to 1.96 L and lowered D_{AV} by ~2.5%. These results show that overly high Penetration rates restrict grout delivery, degrading both the formed diameter and overall formation quality.

3.2.2 Analysis of Penetration Speed on Vertical Bearing Capacity Performance

Figure 15 shows the load-displacement curves for the Penetration speed test group. From Figure 15, it is evident that the overall curve can be divided into three stages: the initial elastic stage, the nonlinear plastic deformation stage, and the failure stage. The ultimate bearing capacity for the PGHP test piles in this batch occurs at the end of the nonlinear plastic deformation stage.

The results of the load-displacement curves for the Penetration speed test group, showing the ultimate bearing capacities of PGHP-DS-1, PGHP-DS-2, and PGHP-DS-3, were 662 *N*, 623 *N*, and 671 *N*, respectively. The results indicate that Penetration speed has a negligible effect on the ultimate bearing capacity of the PGHP piles. This is because Penetration speed mainly affects the cement-soil content and surface roughness of the pile body, factors that have a minor impact on the pile diameter. Since pile diameter is the primary parameter influencing the vertical bearing capacity of the pile foundation, and its variation is limited, the differences in ultimate bearing capacity are small.

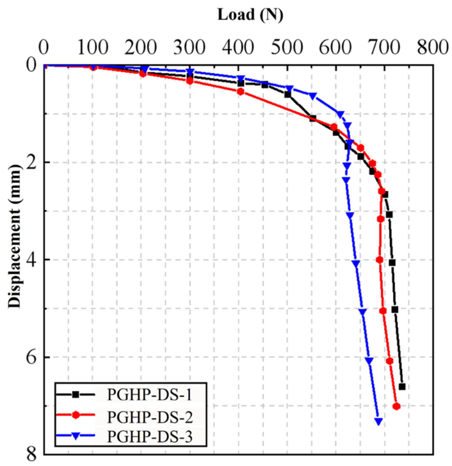

Fig. 15. Load-displacement curve of Penetration speed test group

3.2.3 Analysis of Penetration Speed on Cement-Soil Strength Around the Pile

Figure 16 presents the stud-based measurements for the Penetration-rate series. For all three specimens, the cement–soil strength increases progressively with depth, a pattern attributed to the greater in-situ soil strength at lower horizons and the concomitant rise in resistance to slurry injection, which constrains grout penetration.

The stud point results further show that the mean cement–soil strength S_{AV} declines as Penetration rate increases: for each additional 10 cm·min^{-1}, S_{AV} drops by roughly 12%. The recorded grout intakes were 2.89 L, 2.45 L, and 1.95 L for PGHP-DS-1, PGHP-DS-2, and PGHP-DS-3, respectively. Consistent with these volumes, higher Penetration rates reduce the cement slurry content within the pile body, yielding an inverse relationship between Penetration rate and S_{AV}.

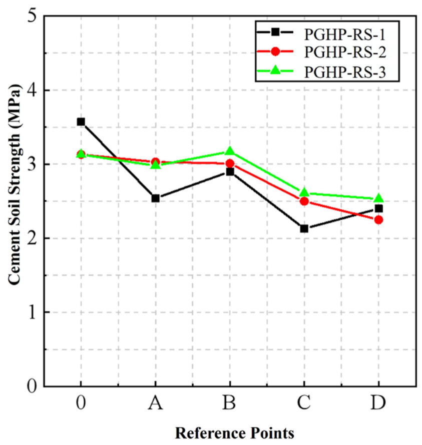

Fig. 16. Cement-soil strength diagram for the Penetration speed test group at nailpoint locations

4 Discussion

The model-scale tests confirmed that simultaneous drilling and pressure grouting effectively produce a continuous soil–cement column around the pile, even in low-permeability soft clay. In tests of this study, the grout column diameter averaged approximately 1.3 times the helix diameter, indicating modest lateral spread. This observation aligns with full-scale excavations of pressure-grouted helical piles (PGHPs) in marine clays, where grout diameters exceeded helix size [13]. Prior small-scale work in soft clays similarly observed grout forming a sleeve with limited radial penetration [14]. Occasionally, a bulb-shaped grout accumulation formed at the pile toe in our tests, consistent with findings where rapid penetration or low mixing energy caused slurry pooling [14]. Laefer et al. [15] reported that strategic placement of grout ports, just below the helix, enhanced confinement and reduced grout waste in sands, suggesting that grout efficiency is highly dependent on delivery configuration. These findings collectively confirm that PGHP can reliably form an enlarged, bonded pile in soft clay, though nozzle design and injection rate must be optimized to prevent uneven column geometry.

The PGHPs in this study had significant enhancement of axial capacity with compressive resistance of about 2.6–2.9 times the compressive resistance of identical ungrouted piles. This 160-190% increase is greater than gains in pre-grouted helical systems where typical capacity improvement is between 80-100% [16, 17]. In Bangkok clay, a composite soil-cement screw pile was shown to have a capacity that is comparable to bored piles, but even higher than conventional helicals[18]. Huang et al. [13] showed an increase of double axial resistance of PGHPs over ungrouted piles in marine clays, with shaft friction contributing almost 75% of the increase. These results con-firm that the cemented soil sleeve has significantly increased the load transfer by skin friction and increased the pile stiffness. The grout not only enhances the effective diameter and interface cohesion but also inhibits the occurrence of buckling by contributing the structural rigidity [17]. These mechanisms taken together mitigate the known limitations of helical piles in soft clay, namely, low shaft friction and susceptibility to slenderness effects.

Preliminary uplift tests also indicated a significant increase in tensile performance. One grouted model showed uplift capacity almost the same as its compressive capacity (within 3%) whereas ungrouted helicals in clay generally have limited uplift resistance [14]. The hardened grout column probably plays a role through (1) increased shaft adhesion and (2) a toe "bulb" that anchors the pile, which was noted in the model-scale study by Zhuang et al. [14]. This is in agreement with other studies by Sakr et al. [19] and Khazaei and Eslami [20] who reported that post-grouting significantly in-creases the tensile and inclined-load capacity in granular soils. Grouted helical piles, therefore, offer a promising solution for applications that require resistance to uplift, such as towers or deep anchors.

Installation parameters were also critical to PGHP performance. The results showed that increasing the number of helix plates improved the uniformity of the column and slightly improved capacity (by 5–15%). Zhuang et al. [14] reported that helices with a large spacing resulted in discontinuous grout coverage resulting in a decrease in available shaft friction. Plate size was another influential factor: doubling the diameter of the helix increased ultimate capacity by about 1.5, mostly by increasing the bonded area. However, over-sizing of the helix without sufficient grout pressure may restrict the formation of the column, as reported by both Zhuang et al. [14] and Mansour and El Naggar [11]. In their study, in-jecting grout upward behind the helix was more effective than injecting from above, which is similar to Perko's earlier recommendation of trailing grout outlets to maximize coverage.

Finally, installation speed was found to have a significant effect on grout intake and load capacity. A slower rate of penetration enabled higher grout uptake, which resulted in thicker columns with a capacity of ~15% greater than that of columns with faster rates [14]. These trends match those of Wang et al. who demonstrated that as feed rate was increased column diameter and interface strength decreased in soft clay[14]. Rotation rate also affected grout distribution: higher torque enhanced mixing of cement and soil and minimized the variability of strength [11, 14]. Collectively, these studies highlight the importance of coordination of control over helix configuration, grout pressure, rotation, and feed rate to guarantee optimal PGHP performance.

5 Conclusion

In this study, the influences of process parameters such as rotational speed and penetration speed on PGHP pile installation process were systematically analyzed through six sets of model pile installation tests, loading tests and stud detection. The differences in bearing performance and PGHP strengths were also investigated. The following are the main conclusions:

(1) Rotational speed: A moderate increase in the rotational speed brings a significant improvement in the uniformity and strength of the PGHPs. The faster the rotational speed, the greater the overall structural integrity of the pile.

(2) Penetration speed: Excessively high Penetration speeds lead to insufficient cement content in the pile, which in turn leads to a decrease in the diameter of the pile and cement-soil strength, thereby weakening the foundation performance of the pile.

These results show the importance of optimizing the process parameters to improve the performance of PGHP piles especially in terms of uniformity, strength between the cement and soil, and the bearing capacity in the vertical direction.

Acknowledgments

This research is funded by "Lianyungang Zhiyuan Electric Power Design CO., LTD. 2025 R&D Services for *Floating Pile Foundation Construction Technology of Transmission Lines in Coastal River Network and Fish Pond Areas*" through grant No. 5210QR250001.

References

1. Cen, H., et al., Bearing performance and failure mechanisms of HSCM piles in marine soft soil under lateral loads. Ocean Engineering, 2024. **313**: p. 119400. DOI: https://doi.org/10.1016/j.oceaneng.2024.119400
2. Liu, H., et al., Analytical approach for vertical dynamic responses of stiffened deep cement mixing pile in unsaturated ground. Soil Dynamics and Earthquake Engineering, 2024. **187**: p. 108969. DOI: https://doi.org/10.1016/j.soildyn.2024.108969
3. Eslami, A., et al., New approach for the numerical analysis of stiffened deep cement mixing columns and piles in coastal engineering through 1D elements. Ocean Engineering, 2024. **313**: p. 119529. DOI: https://doi.org/10.1016/j.oceaneng.2024.119529
4. Rao, S.N., Y.V.S.N. Prasad, and M.D. Shetty, The Behaviour of Model Screw Piles in Cohesive Soils. Soils and Foundations, 1991. **31**(2): p. 35-50. DOI: https://doi.org/10.3208/sandf1972.31.2_35
5. Lutenegger Alan, J., Cylindrical Shear or Plate Bearing? ? Uplift Behavior of Multi-Helix Screw Anchors in Clay, in Contemporary Topics in Deep Foundations. 2012. p. 456-463. DOI: https://doi.org/10.1061/41021(335)57
6. Merifield, R.S., Ultimate Uplift Capacity of Multiplate Helical Type Anchors in Clay. Journal of Geotechnical and Geoenvironmental Engineering, 2011. **137**(7): p. 704-716. DOI: https://doi.org/10.1061/(ASCE)GT.1943-5606.0000478
7. Shao, K., et al., Optimization of inter-helix spacing for helical piles in sand. Journal of Rock Mechanics and Geotechnical Engineering, 2022. **14**(3): p. 936-952. DOI: https://doi.org/10.1016/j.jrmge.2021.11.007
8. Nabizadeh, F. and A.J. Choobbasti, Field Study of Capacity Helical Piles in Sand and Silty Clay. Transportation Infrastructure Geotechnology, 2017. **4**(1): p. 3-17. DOI: https://doi.org/10.1007/s40515-016-0036-0
9. Nabizadeh, F. and A. Janalizadeh Choobbasti, The performance of grouted and un-grouted helical piles in sand. International Journal of Geotechnical Engineering, 2019. **13**(6): p. 516-524. DOI: https://doi.org/10.1080/19386362.2017.1368948
10. Bak, H.M., et al., Axial response and material efficiency of tapered helical piles. Journal of Rock Mechanics and Geotechnical Engineering, 2021. **13**(1): p. 176-187. DOI: https://doi.org/10.1016/j.jrmge.2020.04.007
11. Mansour, M.A. and M.H. El Naggar, Optimization of grouting method and axial performance of pressure-grouted helical piles. Canadian Geotechnical Journal, 2021. **59**(5): p. 702-714. DOI: https://doi.org/10.1139/cgj-2021-0093
12. Farhadian, H. and Z. Maleki, Groutability classification of granular soils with cement grouts. Journal of Rock Mechanics and Geotechnical Engineering, 2023. **15**(6): p. 1580-1590. DOI: https://doi.org/10.1016/j.jrmge.2022.09.007
13. Huang, Y., et al., Axial Behavior of Pressure Grouted Helical Piles Installed in Marine Soft Clay Based on Full-Scale Field Tests. Geotechnical and Geological Engineering, 2022. **40**(12): p. 5799-5812. DOI: https://doi.org/10.1007/s10706-022-02250-2
14. Zhuang, X., et al., Analysis of the installation effect on the axial performance of pressure-grouted helical piles in clay by small-scale model tests. Buildings, 2022. **12**(7): p. 992. DOI: https://doi.org/10.3390/buildings12070992
15. Laefer, D.F., N.E. Menninger, and W.E. Hernandez, Grouting patterns and possibilities with helical piers. 2005. URL: http://hdl.handle.net/10197/2323
16. Vickars Robert, A. and P. Clemence Samuel, Performance of Helical Piles with Grouted Shafts, in New Technological and Design Developments in Deep Foundations. 2012. p. 327-341. DOI: https://doi.org/10.1061/40511(288)23
17. Bagheri, F. and M.H. El Naggar, Effects of installation disturbance on behavior of multi-helix piles in structured clays. DFI Journal - The Journal of the Deep Foundations Institute, 2015. **9**(2): p. 80-91.

DOI: https://doi.org/10.1179/1937525515Y.0000000008

18. Srijaroen, C., et al., Soil–Cement Screw Pile: Alternative Pile for Low- and Medium-Rise Buildings in Soft Bangkok Clay. Journal of Construction Engineering and Management, 2021. **147**(2): p. 04020173. DOI: https://doi.org/10.1061/(ASCE)CO.1943-7862.0001988
19. Sakr, M.A., et al., Behavior of grouted single screw piles under inclined tensile loads in sand. EJGE, 2016. **21**(2016): p. 572-591. URL: https://www.researchgate.net/publication/292131207_Behavior_of_grouted_single_screw_piles_under_inclined_tensile_loads_in_sand
20. Khazaei, J. and A. Eslami, Postgrouted helical piles behavior through physical modeling by FCV. Marine Georesources & Geotechnology, 2017. **35**(4): p. 528-537. DOI: https://doi.org/10.1080/1064119X.2016.1213339